PHYSICAL REVIEW B **69**, 075110 (2004)

Structural, electronic, and magneto-optical properties of YVO_3

A. A. Tsvetkov,* F. P. Mena, P. H. M. van Loosdrecht, and D. van der Marel
Materials Science Center, University of Groningen, Nijenborgh 4, 9747 AG Groningen, The Netherlands

Y. Ren
Experimental Facilities Division, Advanced Photon Source, Argonne National Laboratory, Argonne, Illinois 60439, USA

A. A. Nugroho†
Solid State Chemistry Lab, MSC, University of Groningen, Nijenborgh 4, 9747 AG Groningen, The Netherlands

A. A. Menovsky
Van der Waals–Zeeman Institute, University of Amsterdam, Valckenierstraat 65, 1018 XE Amsterdam, The Netherlands

I. S. Elfimov and G. A. Sawatzky
Department of Physics and Astronomy, The University of British Columbia, 334-6224 Agricultural Road, Vancouver,
British Columbia V6T 1Z1, Canada

(Received 8 April 2003; published 26 February 2004)

Optical and magneto-optical properties of YVO_3 single crystal were studied in the far-infrared, visible, and ultraviolet regions. Two structural phase transitions at 75 K and 200 K were observed and established to be of first and second order, respectively. The lattice has an orthorhombic *Pbnm* symmetry both above 200 K as well as below 75 K and is found to be either dimerized monoclinic $Pb11$ or triclinic $P\overline{1}$ in between. We identify YVO_3 as a Mott-Hubbard insulator with an optical gap of 1.6 eV. The visible spectrum shows three *d*-band excitations at 1.8, 2.4, and 3.3 eV, followed by charge-transfer transitions at about 4 eV. The observed structure is in good agreement with LSDA+U band structure calculations. By using ligand field considerations, we assigned these bands to the transitions to the ${}^4A_{2g}$, ${}^2E_g+{}^2T_{1g}$, and ${}^2T_{2g}$ states. The strong temperature dependence of these bands is in agreement with the formation of orbital order. Despite the small net magnetic moment of $0.01\mu_B$ per vanadium, a Kerr effect of the order of 0.01° was observed for all three *d* bands in the magnetically ordered phase ($T_{\text{Néel}}=116$ K). A surprisingly strong enhancement of the Kerr effect was found below 75 K, reaching a maximum of 0.1°. This effect is ascribed to the nonvanishing net orbital magnetic moment.

DOI: 10.1103/PhysRevB.69.075110 PACS number(s): 71.20.−b, 78.20.−e, 78.30.−j

I. INTRODUCTION

The interplay between the kinetic energy and Coulomb interaction in strongly correlated electron systems enables small external or internal perturbations to manipulate the electronic and magnetic properties of matter. If, in addition, there is a ground-state degeneracy, further interesting phenomena, like an orbital ordering, can arise.[1]

In yttrium orthovanadate, YVO_3, spin and orbital ordering was suggested to be responsible for at least one of the temperature-induced sign reversals of the magnetization.[2] In the magnetically ordered phase, YVO_3 is a canted antiferromagnet, where a net ferromagnetic moment arises due to a small angle between the antiferromagnetically (AFM) oriented spins of the V^{3+} ions. The transition from the room-temperature paramagnetic phase to the antiferromagnetic state occurs at the Néel temperature $T_N=116$ K. Upon further lowering the temperature, the magnetic moment gradually changes sign around 90 K. It has been argued that this magnetization reversal is due to the opposing effects of the Dzyaloshinsky-Moriya interaction and the single-ion magnetic anisotropy on the spin canting direction.[2] The magnetization switches sign again around 77 K. At this temperature the antiferromagnetic order changes from high-temperature *C* type to low-temperature *G* type.[3] A *C*-type AFM order corresponds to an AFM arrangement in planes and a ferromagnetic arrangement between the planes. A *G*-type AFM order implies a completely antiferromagnetic arrangement, both within planes and between them. Ren *et al.*[2] argued that along with the spin order (SO) there is an orbital order (OO) on the vanadium sites. According to the proposed picture, one of two $3d$ electrons always occupies the *xy* orbital, while another electron occupies alternatingly either the *xz* or *yz* orbital on different atoms, thus forming orbital order. In order to minimize the exchange energy a *C*-type spin order is accompanied by a *G*-type orbital order and vice versa. The onset temperature of the orbital order was reported to be much higher than the Néel temperature, $T_{OO}=200$ K.[4]

The proposed picture of the electronic structure still requires confirmation from, for instance, spectroscopic experiments. The strength of optical transitions involving a charge transfer between orbitals of different ions should be highly susceptible to the orbital order between ions. Indeed, one of the aims of the present research is to study the influence of orbital ordering on optical transition strengths and use this technique to study orbital ordering in YVO_3. In this paper we present, among others, optical and magneto-optical measurements of electronic excitations in YVO_3 single crystals.

The observed electronic spectra are discussed using ligand field theory considerations and compared to LDA+U calculations. In addition, magneto-optical Kerr effect experiments are used to elucidate the spin orientation.

The crystal structure of YVO_3 was initially reported to have an orthorhombic *Pbnm* (D_{2h}^{16} in Schoenflies notation) symmetry at all temperatures.[5,6] Recent synchrotron measurements[4,7] report the observation of an additional (401) reflection below 200 K, inconsistent with the *Pbnm* symmetry. The authors concluded[4] that the crystal structure was most likely $P2_1/a$, the highest-symmetry subgroup of *Pbnm*. However, the intensity of the *Pbnm* forbidden reflection was four orders of magnitude weaker than the allowed reflection,[4] which made the refinement of the x-ray data difficult. Far infrared (FIR) spectroscopy is a very sensitive tool to study crystal structure variations. Minor atomic displacements leading to a symmetry breaking, which may be difficult to elicit from x-ray analysis, manifest themselves through the appearance of new phonon lines in the FIR spectrum. Recently, Ulrich *et al.*[8] proposed that YVO_3 may be subjected to a new sort of Peierls instability, where the new ground state involves a dimerization along the *c* axis. From the crystallographic and optical points of view this dimerization removes the inversion center, and IR- and Raman-active phonons become mixed. The *a*-axis-polarized modes stay nevertheless independent from the *b*- or *c*-axis modes if the dimerization affects only the *c* axis. We use FIR vibrational spectroscopy to follow temperature-induced variations of the phonon spectrum and to refine the crystal structure of YVO_3.

II. EXPERIMENTAL DETAILS

The samples were made in a two-stage process. In the first stage a polycrystalline powder of YVO_3 was prepared from YVO_4 powder. The YVO_4 powder was produced by a high-temperature solid-state reaction from appropriate mixtures of predried Y_2O_3 (99.998%) and V_2O_5 (99.995%, metal basis). The oxygen in YVO_4 was reduced by annealing the powder in a flow of pure H_2 at 1000 °C. The second crystal growth stage was carried out by the floating zone technique using a four-mirror furnace in a flow of Ar gas.[9] Single-crystalline boules of about 6 mm in diameter and 60–70 mm in length were obtained from the growth. The crystallinity of the boule used in our experiments was checked by Laue x-ray diffraction. The elemental composition of the crystal was checked using an electron probe microanalyzer (EPMA), and the results showed that the molar ratios were given by $Y:V:O = 1.00:1.00:3.02$. A separate check of the composition using a chemical analysis method showed that the cation ratio of Y over V was 1.00 ± 0.01 and that the oxygen stoichiometry was 3.03 ± 0.02. Both results are in good agreement.

The dielectric function for near-infrared, visible, and ultraviolent spectral ranges was obtained directly by using ellipsometry. Because ellipsometric measurements are very sensitive to contamination of the surface, we used an ultrahigh-vacuum cryostat with a residual pressure less than 10^{-8} mbar. The cryostat was specially designed to minimize the movements of the sample due to the thermal expansion of the cold finger. To minimize the mechanical stress on the windows, the latter were mounted on long stainless steel tubes. The windows were proved to give no artificial effects on the measured spectra at room temperature. The spectra were measured with a VASE32 ellipsometer from J. A. Woollam Co., Inc., covering a spectral range from 6000 cm^{-1} to 36 000 cm^{-1} (0.75–4.5 eV). During the measurements, the samples were aligned in such a way that crystallographic axes were parallel to the normal of the plane of incidence (*y* direction), the normal of the sample surface (*z* direction), and the intersection of these two planes (*x* direction), respectively. Such a symmetrical arrangement simplifies the calculations of the dielectric tensor.[10] The optical response is mainly determined by the *x* component of the tensor. We performed the measurements on a set of samples, where all three crystallographic axes were successively aligned along the *x* direction. Inversion of the ellipsometric data in the assumption of an isotropic sample gives a very good initial approximation for the *x* component of the dielectric tensor. Further refinement of the dielectric tensor is done by an iterative procedure.

Far-infrared and midinfrared reflectivity spectra were measured by Fourier transform infrared reflection spectroscopy using a Bruker IFS-113v. The intensity of the reflected light from the sample was referenced to that from a gold mirror for every measured optical surface at each polarization. The sample was mounted on the cold finger of a helium flow cryostat, whose temperature was varied from 300 K down to 4.2 K. Kramers-Kronig transformation was used to calculate the dielectric function and optical conductivity from the reflectivity data in the infrared region. For these calculations we extrapolated the reflectivity below 50 cm^{-1} with a pure ionic insulator response. For the high-frequency extrapolation we used the reflectivity calculated from the ellipsometric data.

The magneto-optical properties were measured using a homebuilt Kerr spectrometer. We used an electro-optical modulation technique, similar to Ref. 11, to obtain simultaneously the Kerr rotation and ellipticity induced by the sample. The combination of a xenon arc lamp, the windows, a Si detector, and other optical components limited our spectral range to 350–800 nm (1.55–3.5 eV).

III. STRUCTURAL PHASE TRANSITIONS

The orthorhombic *Pbnm* crystal structure of YVO_3 is shown in Fig. 1. It can be considered as a distorted perovskite structure. When compared to the perovskite unit cell, the orthorhombic *a* and *b* axes lay along the diagonals of the perovskite unit cell and the corresponding translational vectors are approximately $\sqrt{2}$ times longer. The *c*-axis dimension of the orthorhombic unit cell is twice as large. The YVO_3 unit cell contains thus four formula units. Vanadium ions have an octahedral surrounding. The octahedrons are distorted, rotated, and tilted with respect to each other, as illustrated in Fig. 1.

In the present work we use optically active phonons to track changes in the crystal symmetry. As yttrium orthovanadate is an insulating compound, its optical response in the FIR region is determined purely by lattice vibrations. In Fig.

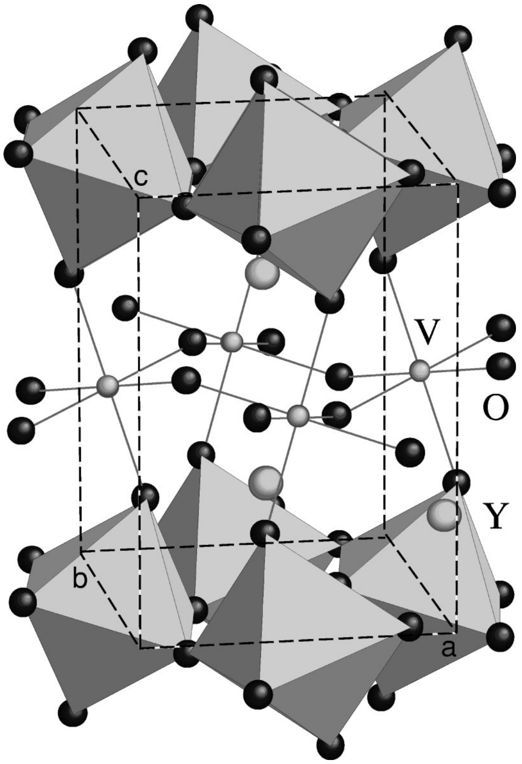

FIG. 1. *Pbnm* orthorhombic crystal structure of YVO_3.

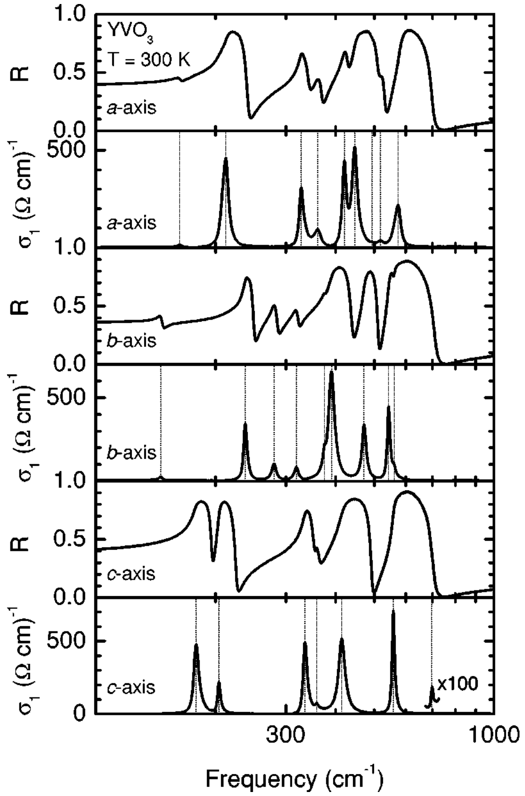

FIG. 2. Room-temperature reflectivity and corresponding optical conductivity for the three crystallographic directions. Dashed lines indicate positions of the phonon modes. There are nine, nine, and seven modes for the *a*, *b*, and *c* axes, respectively, in agreement with the *Pbnm* symmetry.

2 the room-temperature reflectivity for all three polarizations is shown together with the optical conductivity. As can be seen, there are nine, nine, and seven optically active modes for the *a*, *b*, and *c* axes, respectively. The positions of the TO phonon frequencies are shown by vertical lines and the frequencies are given in Tables I and II. Some resonances are very weak. For example, the mode of highest frequency for the *c* axis is hardly visible in the conductivity and appears as a shoulder on the reflectivity curve. It gains intensity as the temperature is lowered and reaches its maximum in the low-temperature orthorhombic phase. Shown in Fig. 3 is the temperature dependence of the reflectivity for all three polarizations. The number of the phonons stays the same between room temperature and 200 K. Below 200 K a number of additional phonons gradually emerge. We illustrate this by picturing some of the new modes for the *b* and *c* axes in Fig. 4. As can be seen from the figure, the intensity of the new modes evolves continuously and monotonically as the temperature decreases, reaching its maximum at 75 K. The optical strengths remain, however, one or two orders of magnitude weaker than that of the original main modes. Below 75 K the new phonons discontinuously disappear. As an example, the temperature dependence of the oscillator strength of the new 522 cm^{-1} mode is shown in Fig. 4.

To analyze the observed phonon spectra, we apply a group theory analysis. The primitive cell of YVO_3 contains four formula units, yielding 60 phonon modes in total. In the *Pbnm* lattice the four yttrium atoms and four vanadium atoms occupy equivalent sites $4c$ and $4b$ in Wyckoff notation with site symmetry C_s^{xz} and C_i, respectively. The 12 oxygen atoms are distributed between two inequivalent sites $4c$ and $8d$ with site symmetry C_s^{xz} and C_1, respectively. Using the usual procedure,[12] we find that the phonon normal modes transform according to

$$\Gamma = 7A_g + 8A_u + 5B_{1g} + 10B_{1u} + 7B_{2g} + 8B_{2u} + 5B_{3g} + 10B_{3u}.$$

The total representation Γ can be subdivided into three acoustic vibrational modes $B_{1u}+B_{2u}+B_{3u}$, 24 Raman-active modes $7A_g+5B_{1g}+7B_{2g}+5B_{3g}$, eight silent A_u

TABLE I. TO phonon modes for the *a* and *b* axes at room temperature.

B_{1u} (a)			B_{3u} (b)		
ω (cm^{-1})	γ (cm^{-1})	S_a	ω (cm^{-1})	γ (cm^{-1})	S_b
162.2	3.2	0.08	144.3	15.5	0.73
211.6	8.5	5.4	237.4	5.5	2.0
328.5	9.9	1.6	280.1	8.4	0.64
359.2	15.0	0.56	318.7	7.8	0.35
420.8	10.4	1.4	374.5	6.3	0.22
446.8	17.3	2.6	390.7	16.5	4.21
494.5	10.0	0.005	471.7	13.3	1.2
517.5	15.5	0.06	543.7	9.8	0.86
572.4	22.6	0.91	559.8	17.5	0.21

TABLE II. c-axis phonons at 75 K. B_{2u} modes originate from the room-temperature phase. New vibrational modes, appearing below 200 K, are designated as A.

Mode	Frequency	S_a	S_b	S_c
B_{2u}	**180.2**	-	-	7
A	199	-	0.037	0.008
B_{2u}	**205.6**	-	0.006	0.78
B_{2u}	**333.0**	0.19	0.008	2.9
A	350	-	0.67	0.003
B_{2u}	**359.8**	-	0.02	0.37
B_{2u}	**420.5**	1.6	0.076	1.6
A	522	-	0.024	0.018
B_{2u}	**564.9**	-	0.014	1.2
B_{2u}	**699.2**	-	-	0.002

modes, and 25 infrared-active modes. The infrared vibrations are split into $9B_{1u}(E||a)$, $9B_{3u}(E||b)$, and $7B_{2u}(E||c)$ modes with the electric dipole moment aligned along the a, b, and c axes, respectively.

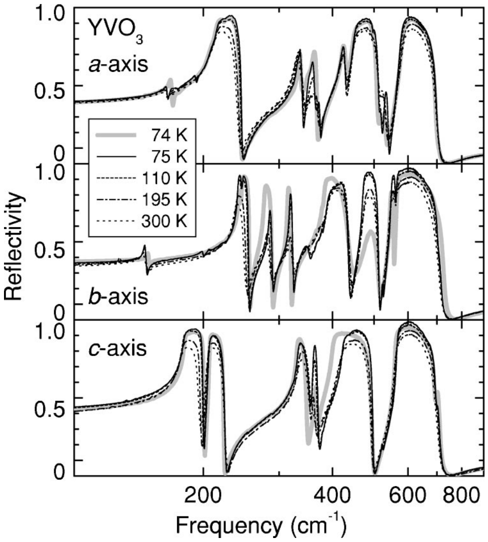

FIG. 3. Temperature dependence of the FIR reflectivity for three polarizations.

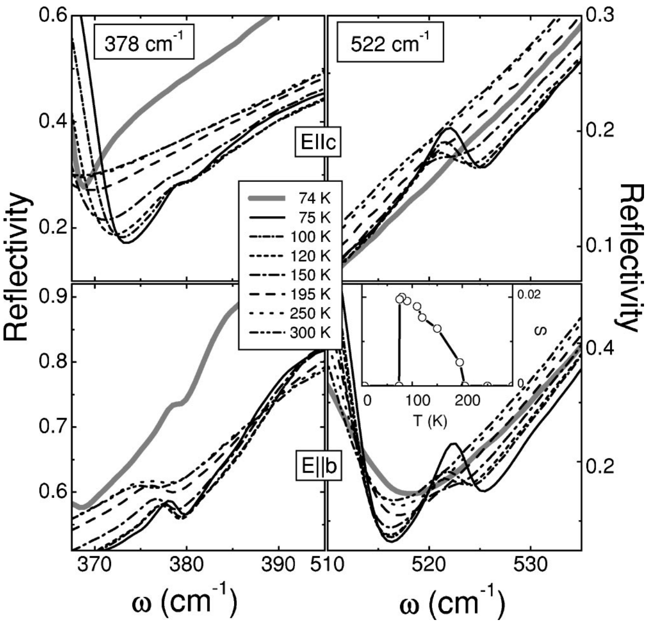

FIG. 4. Left panels: "leakage" of the b-axis B_{3u} mode into the c-axis response. Right panels: appearance of a new previously silent A_u mode in the b and c responses. Inset: temperature dependence of the optical strength of the new mode.

A similar group theory analysis is applied to the lower-symmetry structures $P2_1/a$, $P\overline{1}$, and $Pb11$, which are subgroups of the $Pbnm$ symmetry. Table III illustrates which symmetry elements are inherited in different symmetries. We also show the relation between the widely used notation $Pbnm$, adopted also in this paper, and the standard notation $Pnma$. The monoclinic $P2_1/a$ symmetry is postulated from x-ray measurements.[7] The triclinic $P\overline{1}$ symmetry, second highest possible symmetry after $P2_1/a$, was proposed by us based on indications that the center of inversion is conserved.[13] Both x-ray[7] and optical[13] measurements show that the symmetry cannot be higher than monoclinic. Recent neutron experiments indicated the possibility of a dimerized state.[8] Dimerization displaces the middle VO$_2$ plane (see Fig. 1) away from its central position. It removes the inversion center and screw axis from the symmetry operations of $P2_1/a$. The remaining symmetry group includes only a glide plane **b** and is referred to as $Pb11$.

As the x-ray measurements do not reveal any multiplication of the unit cell,[4] the number of atoms in the unit cell is not changed. For monoclinic $P2_1/a$ (C_{2h}^5) symmetry group one expects $16B_u$ IR-active and 2 acoustic modes in the bc plane and one acoustic and $17A_u$ IR modes along the a axis. In the case of triclinic $P\overline{1}$ (C_i^1) symmetry, there should be $33A_u$ IR modes, which can have components along all three axes. Monoclinic $Pb11$ (C_s^2) symmetry splits phonons into two irreducible representations $30A'(E||bc)+30A''(E||a)$, where Raman and IR modes are mixed. How the phonon mode irreducible representations transform into each other due to the descent in symmetry is depicted in Fig. 5. Both monoclinic C_{2h}^5 and triclinic C_i^1 crystal lattices have an in-

TABLE III. Possible symmetries and symmetry operations in the intermediate phase (75 K$<T<$200 K).

N	$Pnma$	$Pbnm$	$P2_1/a$	$P\overline{1}$	$Pb11$
	D_{2h}^{16}	D_{2h}^{16}	C_{2h}^5	C_i^1	C_s^2
(1)	1	1	1	1	1
(2)	$2(0,0,\frac{1}{2})\frac{1}{4},0,z$	$2(\frac{1}{2},0,0)x,\frac{1}{4},0$	2_1	-	-
(3)	$2(0,\frac{1}{2},0)0,y,0$	$2(0,0,\frac{1}{2})0,0,z$	-	-	-
(4)	$2(\frac{1}{2},0,0)x,\frac{1}{4},\frac{1}{4}$	$2(0,\frac{1}{2},0)\frac{1}{4},y,\frac{1}{4}$	-	-	-
(5)	$\imath$	$\imath$	$\imath$	$\imath$	-
(6)	$\mathbf{a}x,y,\frac{1}{4}$	$\mathbf{b}\frac{1}{4},y,z$	**b**	-	**b**
(7)	$\mathbf{m}x,\frac{1}{4},z$	$\mathbf{m}x,y,\frac{1}{4}$	-	-	-
(8)	$\mathbf{n}(0,\frac{1}{2},\frac{1}{2})\frac{1}{4},y,z$	$\mathbf{n}(\frac{1}{2},0,\frac{1}{2})x,\frac{1}{4},z$	-	-	-

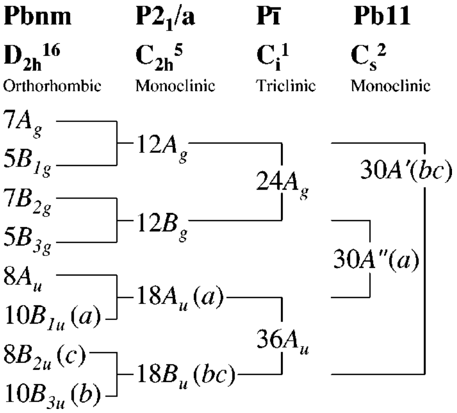

FIG. 5. Transformations of the phonon irreducible representations due to the descent in lattice symmetry.

version center. As a result the IR and Raman modes do not mix with each other for these symmetries. In point group C_{2h}, because the b and c axes are not orthogonal anymore, the corresponding phonons mix and form the B_u representation $7B_{2u}+9B_{3u}\rightarrow 16B_u$. The mode A_u, silent in D_{2h}^{16} symmetry, becomes optically active and together with the B_{1u} mode gives the A_u representation $8A_u+9B_{1u}\rightarrow 17A_u$. A possible twinning in the b-c plane cannot be a reason for leaking the b-c phonons to the a axis and vice versa. Alternatively, in the lowest C_i^1 symmetry all the phonons mix together, as seen in Fig. 5. In the $Pb11$ symmetry, Raman A_g modes become visible in the bc plane and together with the IR B_u phonons form the A' representation $12A_g+18B_u \rightarrow 30A'$. Similar, Raman B_g modes can be observed in the a-axis response together with IR A_u modes $12B_g+18A_u \rightarrow 30A''$. An important difference between $P\overline{1}$ and $Pb11$ symmetries is that in $P\overline{1}$ the same modes can be observed in all three polarizations, while in $Pb11$, a eigenmodes on one side and b and c eigenmodes on the other side remain separate.

At room temperature we observed nine, nine, and seven phonons for the a, b, and c axes, respectively (see Fig. 2). The TO phonon frequencies ω, broadening Γ, and optical strength S are presented in Tables I and II. Our observation confirms the orthorhombic *Pbnm* symmetry of the crystal lattice at room temperature. At lower temperatures, as far as the crystal structure is concerned, we can conclude from Fig. 4 that the *Pbnm* symmetry is transformed to a lower one below 200 K and is restored again below 75 K. The temperature evolution of the optical strength of the new phonons indicates that the phase transition at 200 K has a second-order nature and that the one at 75 K has a first-order nature. Shown in Table II are the phonon mode frequencies and strengths observed in the c-axis spectrum at 75 K. The lines active also in the high-temperature phase are in boldface and assigned to B_{2u}; those appearing only in the intermediate temperature phase are labeled by A. Although much more new phonons are seen for all three axes, only the activated c-axis modes, having a counterpart in the other axes, are shown in the table. First, one can see that the original c-axis phonon lines give rise to phonon absorptions along the b axis. The reverse is also valid. The phonons from the b axis "leak" in the intermediate phase to the c axis, which is shown in Fig. 4. This agrees with all three symmetries under consideration. However, there are a number of newly activated absorption peaks (199, 350, and 522 cm^{-1}) in the b and c polarizations, which do not have parents in other polarizations. The fact that these new modes are exactly at the same frequency in both b and c polarizations—as shown in the right panels of Fig. 4—excludes the possibility of the doubling of the unit cell as their origin. The appearance of new modes is forbidden in the $P2_1/a$ symmetry (see also Fig. 5). This observation rules out $P2_1/a$ symmetry for the intermediate phase. Because these modes are not seen in any polarization above 200 K or below 75 K, we can ascribe these phonons either to the previously silent mode A_u activated in $P\overline{1}$ symmetry or to the high-temperature Raman modes activated in $Pb11$ symmetry. We did not observe any correlation of phonons between b and c on the one side and a on the other side, apart from the modes already present both in a and c polarizations above 200 K (333 and 420 cm^{-1} modes in Table II). This could imply that the triclinic distortions are extremely small, in particular for the a axis. However, the $Pb11$ symmetry gives a more natural explanation, as it keeps the a and bc modes apart, consistent with the observation. All in all, these facts draw us to the conclusion that the crystal structure of YVO$_3$ in the intermediate phase most likely has a monoclinic $Pb11$ symmetry. A further test of this conclusion could be a comparison to Raman measurements, when data become available.

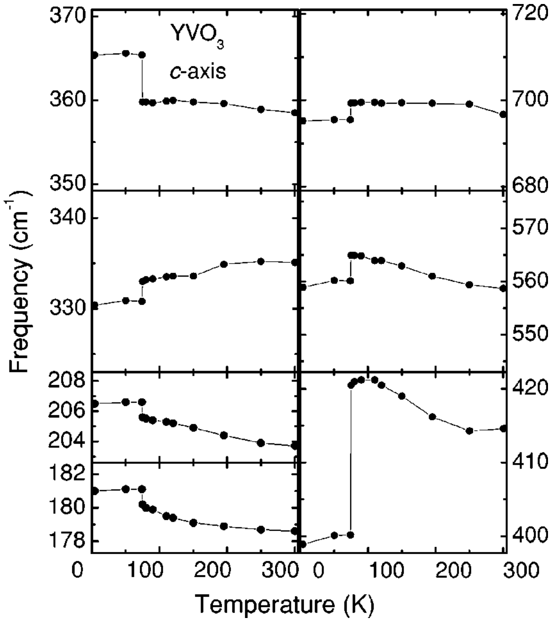

FIG. 6. Temperature dependence of the TO frequencies for the c-axis B_{2u} phonon modes. For comparison purposes, the vertical scale in each square comprises 6% of the central frequency.

Finally, we remark on the relation between the electronic and crystal structure changes. From Fig. 6 one can see that the main modes evolve smoothly through the second-order

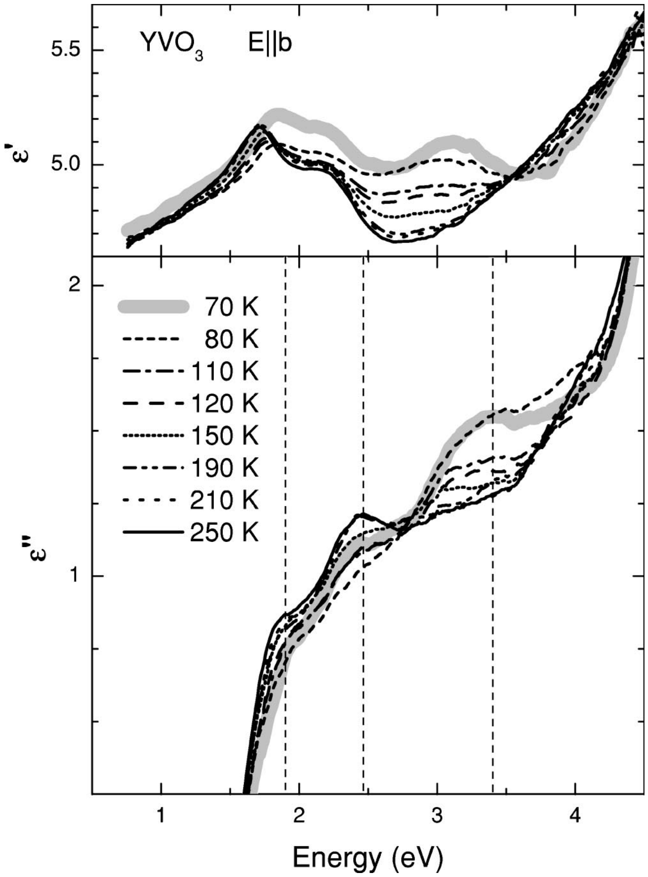

FIG. 7. Temperature dependence of the real and imaginary parts of the b-axis dielectric function for YVO_3. The vertical lines indicate locations of the band maxima.

phase transition, where the appearance of orbital order is reported.[4,7] However, a number of phonon frequencies change substantially at the first-order phase transition, where spins and orbitals switch their ordering. The frequency change is found to be particularly strong for the modes around 400 cm^{-1}. From lattice dynamical calculations[14] for the isostructural compound $LaMnO_3$ we conclude that the 400 cm^{-1} modes mainly involve vanadium-oxygen bond vibrations. Therefore, it seems that the main structural changes at the first-order transition involve a distortion of the VO_6 octahedra.

IV. ELECTRONIC STRUCTURE

The yttrium Y^{3+} and vanadium V^{3+} ions in YVO_3 both carry a formal charge 3+. Yttrium has a complete shell, and it can be excluded from consideration for the electronic transitions. Vanadium has two 3d electrons in the outer shell. We can thus expect two types of optical transitions in the visible range: d-d transitions between vanadium ions with the characteristic energy of the Mott-Hubbard gap [Mott-Hubbard (MH) transitions] and the charge-transfer (CT) transitions from the oxygen 2p band to the free states in the vanadium 3d band.

Shown in Figs. 7 and 8 are the real and imaginary parts of the YVO_3 dielectric function, $\varepsilon=\varepsilon'+i\varepsilon''$, measured at various temperatures. The optical response at low temperatures is determined by three bands with their maxima located at 1.8, 2.4, and 3.3 eV, followed by a sharp upturn above 4 eV. The optical gap is found at 1.6 eV. It is quite remarkable to observe that the intensity of some bands, located in the region of a few electron volts, changes by as much as 50% for temperature variations as small as $k_BT \leqslant 26$ meV.

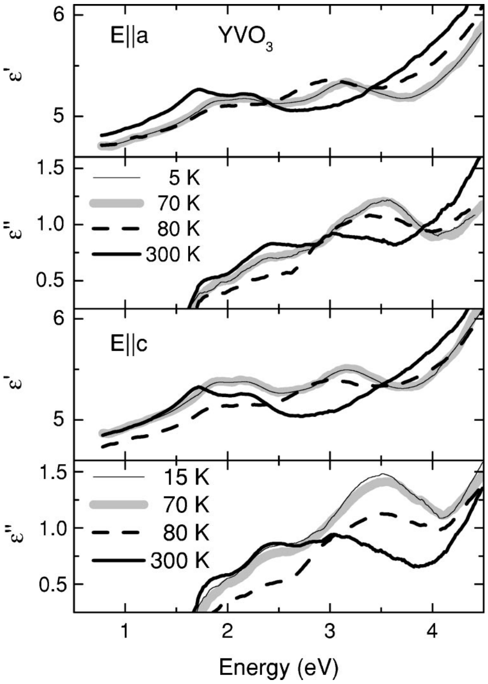

FIG. 8. Real and imaginary parts of the dielectric function for the a and c axes of YVO_3.

Recently Miyasaka *et al.*[15] reported reflectivity measurements on YVO_3, where the optical conductivity, obtained through the Kramers-Kronig relations, revealed only two peaks. Also the temperature dependence and the reported anisotropy of the conductivity were different. Since ε'' is approximately 5 times smaller than ε' in the visible part of the spectrum, the reflectivity is mainly determined by the real part of ε. The d-band structure in ε' and ε'' gives rise to reflectivity variations of only a few percent and the temperature-induced changes of the reflectivity are around 1% or less. This together with the close vicinity of the strong charge-transfer transitions places heavy demands on the accuracy of the measurements. A small error can substantially affect an interpretation of the electronic spectrum. Therefore, we used the ellipsometry technique to determine ε' and ε'' directly at each particular photon energy, excluding the necessity of reference measurements. In addition we took special precautions to perform measurements in ultrahigh vacuum in order to avoid surface contamination at low temperatures. We trust that these measures substantially minimize a possible error.

Let us first discuss the origin of the bands. Following the general classification scheme,[16] YVO_3 is a Mott-Hubbard insulator. The lowest excitations are $d_i^2 d_j^2 \rightarrow d_i^3 d_j^1$ transitions

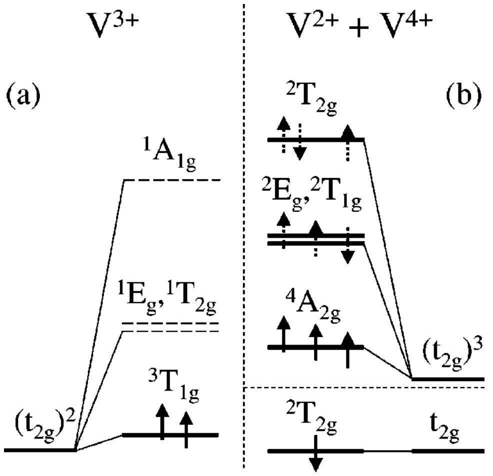

FIG. 9. Energy diagram for (a) the ground state of the vanadium ions and (b) excited states of two vanadium sites.

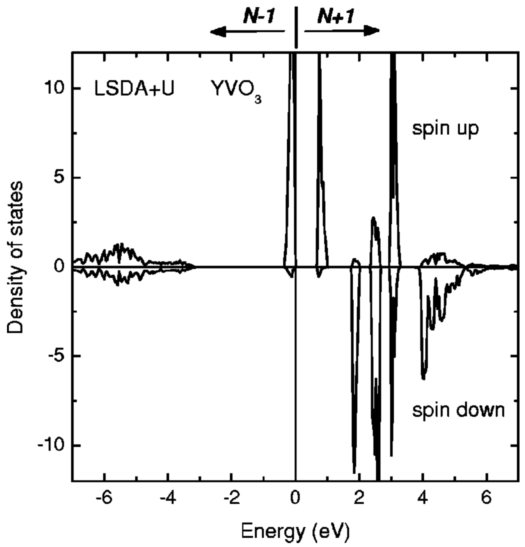

FIG. 10. Vanadium $3d$ partial density of states for spin-up and spin-down electrons, obtained in local spin-density approximation with the Hubbard potential U taken into account. $N-1$ and $N+1$ correspond to the electron removal and electron addition states, respectively.

between different vanadium ions, i and j. The upturn above 4 eV is due to charge-transfer excitations. This general picture also follows from our LSDA+U calculations and agrees with previous room-temperature measurements.[17,18] The fine structure of the MH band observed here has not been reported previously and will be discussed using ligand field theoretical considerations and LSDA+U calculations.

Because the orthorhombic distortion of the oxygen octahedron is small, we can neglect any on-site d-d excitations. For the same reason we can, considering the energy diagram, restrict ourselves in the first approximation to O_h symmetry on the vanadium site. The e_g orbitals can be excluded, because due to the large crystal field splitting, $10Dq$, the mixing between e_g and t_{2g} orbitals is expected to be small. Thus, in the strong-field approximation the two d electrons occupy t_{2g} orbitals.

If we take into account the Coulomb interaction, the t_{2g} level is split into $^3T_{1g}$, ^1E_g, $^1T_{2g}$, and$^1A_{1g}$ levels, as shown in Fig. 9(a). The ^1E_g and $^1T_{2g}$ levels are degenerate in the O_h symmetry. In the ground state the d electrons occupy the lowest-energy $S=1$ state $^3T_{1g}$, in agreement with Hund's rules. The MH excitations occur from the initial state with two vanadium atoms in the d^2 state to the final state with the first atom in the d^1 (V^{4+}) and the second in the d^3 (V^{2+}) states. In the final state the wave function of the single electron follows obviously only one irreducible representation $^2T_{2g}$, while the d^3 state splits into four levels $^4A_{2g}$, ^2E_g,$^2T_{1g}$, and $^2T_{2g}$, with ^2E_g and $^2T_{1g}$ again being degenerate. The energy diagram of the final state is depicted in Fig. 9(b). The three observed bands in Fig. 7 correspond to transitions to these three energy levels. According to the measurements, these bands span the energy range of 1.5 eV from 1.8 eV to 3.3 eV. With the crystal field splitting of $10Dq \approx 2$ eV, our assumption of a small admixture of e_g orbitals is justified.

The picture obtained with the ligand field theory is in good agreement with our LSDA+U calculations. LSDA+U band structure calculations have been performed in the linear muffin-tin orbital (LMTO) calculation scheme.[19,20] Vanadium $3d$ partial densities of states were obtained in the LDA+U calculation with $U=3.4$ eV and $J=0.85$ eV for the low-temperature crystal and magnetic structure of YVO_3. The results are consistent with previous calculations of the electronic structure.[21] As can be seen from the electron density of states in Fig. 10, the highest occupied states form a narrow d band, with both electrons in a spin-up state. The AFM-ordered neighboring vanadium ion should accordingly be in a spin-down state. The lowest unoccupied band corresponds to the addition of an electron with spin up. This agrees with the lowest excited $^4A_{2g}$ state, which indeed puts electrons in the high-spin state $S=3/2$. Two consequent excitation bands are formed by the transfer of spin-down electrons, again in agreement with the low $S=1/2$ spin states in the ^2E_g, $^2T_{1g}$, and $^2T_{2g}$ representations found from the ligand field theory. Higher electron-addition bands with equal spin-up and spin-down populations have an e_g origin. From the energy distribution of the bands in Fig. 10 one can see that YVO_3 is indeed a Mott-Hubbard insulator.[16] The lowest excitations are d-d transitions $d^2d^2 \rightarrow d^3d^1$. The charge-transfer transitions $d^2 \rightarrow d^3\overline{L}$ occur at higher energies than the d-d transitions.

The temperature dependence of the optical response of YVO_3 is shown in Figs. 7 and 8. There is only a small temperature dependence between 70 K and 5 K, as can be seen in Fig. 8, and the corresponding data are omitted in the further consideration. To clarify the temperature dependence of the MH bands, Fig. 11 shows a differential dielectric function for $E||b$, where the 250 K data are subtracted from the curves in Fig. 7. In order to quantify temperature variations of the optical strength of the bands, we fitted simultaneously the real and imaginary parts. The differential dielectric function turned out to be well fitted with three Gaussians in the imaginary part and with its Hilbert transform, the Dawson

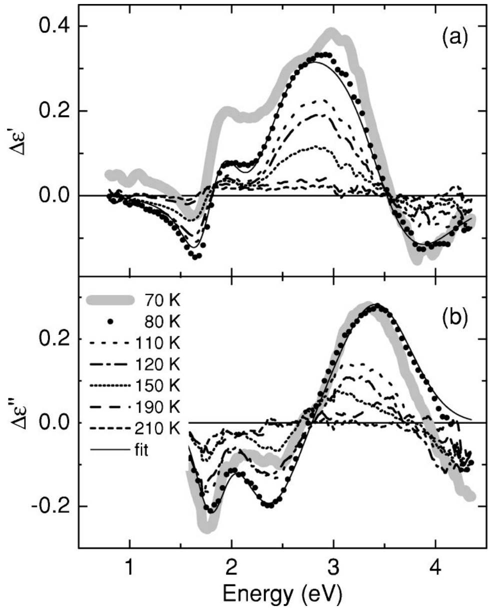

FIG. 11. The dielectric functions from Fig. 7 after subtraction of the 250 K data. The fit curve shows a simultaneous fit to the real and imaginary parts for the 80 K data.

function, in the real part. The fitted curves for 80 K are shown along with the experimental data in Fig. 11. The full dielectric function shown in Fig. 7 was also fitted in the same way, but an additional fourth Gaussian was necessary to account for the CT band. In this way the position of the bands was confirmed to be temperature independent. However, it was not possible to determine accurately the absolute optical strength of the MH bands due to an additional non-Gaussian contribution. It was also impossible to determine the position of the 3.3 eV band at high temperatures because of its vanishing presence in the spectra. The band positions and optical strengths obtained from the fits are plotted in Fig. 12. The dielectric function reveals minimal variations between room temperature and the second-order structural phase transition at 200 K. Below 200 K a strong growth of the 3.3 eV band is observed, which is accompanied by a decrease of the 1.8 and 2.4 eV bands. The total integrated change of the optical strength of these MH bands remains virtually zero down to the Néel temperature $T_N=116$ K. In the magnetically ordered state the 3.3 eV band acquires additional strength. The additional spectral weight transfer should come from higher energies, most probably from the e_g states, as the decrease of the low-energy bands cannot account for it. Indeed, the lowest-energy state in the $t_{2g}^2e_g$ configuration is obtained by adding an e_g electron to the ground state $^3T_{1g}$. Four irreducible representations, $^4T_{1g}$, $^4T_{2g}$, $^2T_{1g}$, and $^2T_{2g}$ can be formed from this configuration, where the latter representation descends also from the t_{2g}^3 configuration. Antiferromagnetic order favors transitions to the low-spin states and thus gives additional optical strength to the $^2T_{2g}$ state.

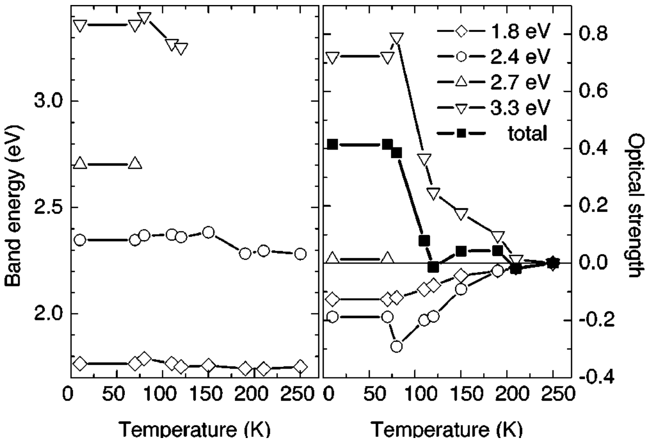

FIG. 12. Temperature dependence of the position of the electron bands (left) and their optical strength together with the total spectral weight of the three bands (right).

At the first-order phase transition, the optical strength of the 2.4 and 3.3 eV bands experiences jumps in opposite directions. Additionally, as can be seen in Fig. 11(a), a new shoulder emerges at around 2.7 eV. This appears in Fig. 7 as an extended flat region, which becomes visible probably due to the narrowing of the 3.3 eV band. However, its optical strength is very small.

The optical spectrum begins to change below the second-order phase transition at 200 K. These changes cannot be directly related to the lower symmetry as the 3.3 eV band does not disappear in the low-temperature orthorhombic phase. The reason should rather come from some electronic correlations and associated distortions of the VO_6 octahedrons. Ren *et al.*[2] suggested that the spin order in YVO_3 is accompanied by an orbital order. The orbital order is reported to appear below the 200 K phase transition.[4,7] In the proposed picture for the orbital ordering, the *xy* orbitals are always occupied by one of the two *d* electrons, while the occupation of the *xz* and *yz* orbitals alternates in an AFM order. The orbital order was found to be different above and below 77 K in agreement with the different magnetic order. According to Ren *et al.*,[2] there is a *C*-type magnetic and *G*-type orbital order above 77 K and a *G*-type magnetic and *C*-type orbital order below 77 K.

We now turn to a discussion of how orbital and magnetic ordering influences the optical conductivity. We consider a model where the optical conductivity is proportional to the electron transition probability between two neighboring vanadium sites. There are in total nine independent eigenfunctions in the $^3T_{1g}$ representation. At room temperature the electron transition probability can be calculated by averaging over arbitrary orientations of spins and orbits on two ions—i.e., by averaging over all linear combinations of these nine wave functions. Magnetic or orbital order limits the choice of initial wave functions. At lower temperatures we can expect that the electron transition from the $S=1$ state on the first ion to the $S=3/2$ state on the other ion becomes less probable due to the antiferromagnetic order. Thus, the intensity of the lowest band should decrease. As can be seen from Figs. 7 and 11, the optical strength of the lowest band indeed decreases upon cooling. By using a more rigorous analysis of the transition probabilities, we can evaluate if a particular order is consistent with the observed temperature dependence of $\varepsilon(\omega)$. In this analysis we neglect the tilting of the

TABLE IV. Calculated transition probabilities at room temperature, in the AFM spin-ordered (SO) state and in the AFM spin- and orbital-ordered (SO-OO) state.

Order	$^4A_{2g}$	$^2E_g+{}^2T_{1g}$	$^2T_{2g}$
Room temperature	0.49	0.84	0.44
AFM SO	0.30	1.48	0.89
AFM SO-OO	0.33	1.67	1.0

octahedra and assume that the transition integrals between *d* orbitals on the neighboring vanadium ions are the same for all directions and for all *d* orbitals. The conductivity is assumed to be determined by the probabilities to create a pair consisting of an occupied orbital on one site and an empty orbital on the neighboring site, with the constraint that the transition be allowed. The intersite *d*-*d* transitions are mediated by the *p* orbitals of the oxygen ions between the vanadium sites. At room temperature all $^3T_{1g}$ states are occupied randomly. At lower temperatures we used the magnetic and orbital order, suggested above.[2] If we assume the transition integral from completely occupied to completely empty orbital as unity, then the transition probabilities at room temperature are found to be 0.49, 0.84, and 0.44 for the $^4A_{2g}$, $^2E_g+{}^2T_{1g}$, and $^2T_{2g}$ final states, respectively. We also calculated the transition probabilities for AFM spin order and for AFM spin order accompanied by the aforementioned orbital order (see Table IV). Both simple AFM-SO and AFM-SO+OO lead to a decrease of the lowest band and an increase of the intensity of the highest band, consistent with the observations.

However, none of the considered orderings gives the correct sign for the intensity change for the middle band—i.e., a decrease of strength with decreasing temperature. Moreover, we found that no combination of completely polarized states ($S_z=1$) can give the desired intensity decrease for the $^2E_g + {}^2T_{1g}$ band. The same conclusions hold if the on-site symmetry is lowered to tetragonal. If some addition of the $S_z=0$ initial wave function is allowed, as suggested by neutron measurements,[4] a large variety of possible orbitally ordered structures becomes allowed. Although different orbital orderings can indeed explain the observed intensity changes, it is not possible to give a preference to a particular order.[22]

V. MAGNETO-OPTICAL KERR EFFECT

The energy diagram shown in Fig. 9 was derived assuming a local cubic symmetry on the vanadium site. In reality, one axis of the octahedron is different from the other two. This tetragonal-type distortion additionally splits the multiplet structure, which partially lifts the degeneracy of the ground and excited states. On top of that, a spin-orbital coupling provides segregation of the states by the quantum number M_J. The latter gives rise to the magneto-optical Kerr effect (MOKE). The temperature dependence of the Kerr rotation spectrum $\Theta_K(E)$ is shown in Fig. 13. The curves are shifted for clarity. The measurements were performed in the polar geometry at nearly normal angle of incidence, with a magnetic field of 0.1–0.2 T parallel to the *a* axis, $H||a$. In the other field orientations, the magnetic moment was too small for the Kerr rotation to be detected. No rotation of the polarization plane was observed above the Néel temperature within our experimental error. Below the Néel temperature but above the first-order phase transition, only a weak structure of the order of $\Theta_K\approx 0.01°$ can be seen. Below 75 K a remarkable peak as large as $\Theta_K=0.1°$ is observed. In total, there are three resonance structures. Enlarged in the inset of Fig. 13 are two surprisingly narrow dispersion-type resonances at 1.8 and 2.2 eV that have positions approximately corresponding to the onset of the two first MH bands. Their intensity, though rather small $\sim 0.01°$, is well reproduced on different samples. The third broad peak appears to have maximum at 3.5 eV, which is also confirmed by the zero crossing of the Kerr ellipticity $\varepsilon_K(E)$. This band lies below the charge-transfer onset and corresponds to the *d*-*d* transitions. The maximum rotation in this band amounts to $\sim 0.1°$. Such a large magneto-optical effect seems to be quite surprising, because from the electrodynamics point of view the time-reversal symmetry, although broken on the microscopic scale, is usually restored on the macroscopic scale in antiferromagnetic compounds. If this indeed were the case in YVO_3, the Kerr rotation would mainly result from the small 0.2° spin canting and would be as minuscule as the net magnetic moment is. For comparison, the saturation magnetic moment in Ni is $0.61\mu_B$ per atom—i.e., approximately 60

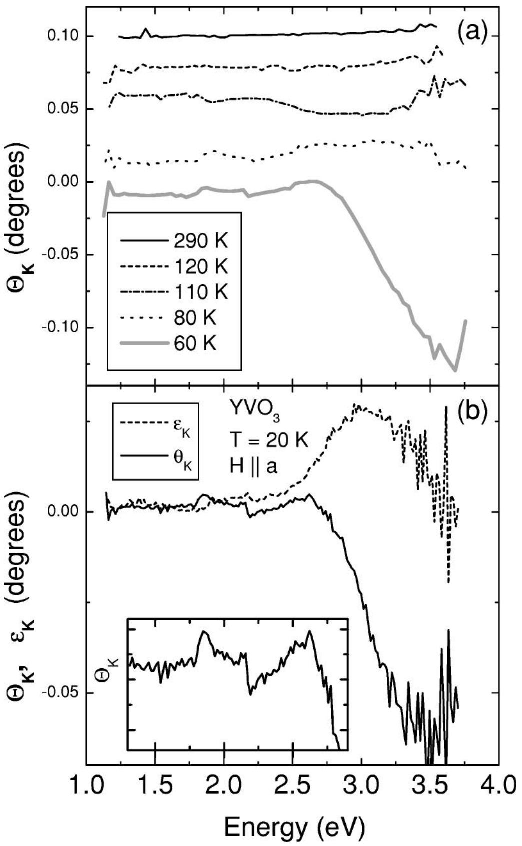

FIG. 13. (a) Temperature dependence of the Kerr rotation measured in the polar geometry with $H||a$. (b) The Kerr rotation Θ_K together with the Kerr ellipticity ε_K in the low-temperature phase. Inset: enlarged view of the resonances at 1.8 and 2.2 eV.

times larger that the net moment of 0.01 Bohr magneton per vanadium atom in YVO_3. Still the Kerr rotation in Ni is quite comparable to those of the low-temperature phase of YVO_3 and lies between 0.1° and 0.2° in the visible range.

Antiferromagnetic compounds can have large magneto-optical effects, as was shown recently,[23,24] if the local spin and orbital magnetic moments are not collinear. In particular, an orbital magnetic moment does not vanish in transition-metal perovskites with the *Pbnm* structure due to the tilting of the octahedra.[25] We can find nonvanishing ferromagnetic components of the net orbital magnetic moment $\mathbf{M}_L$ from symmetry considerations, following the guideline and notations from Ref. 25. There are four inequivalent vanadium sites $i=1,2,3,4$ in the YVO_3 unit cell. These sites can be generated by four symmetry transformations, unity operation E, and three screw axes, S_{2x} with the shift $(\frac{1}{2},0,0)$ and coordinates $x,\frac{1}{4},0$; $S_{2y}(0,\frac{1}{2},0)$ $\frac{1}{4},y,\frac{1}{4}$; and $S_{2z}(0,0,\frac{1}{2})$ $0,0,z$. Here x, y, and z are parallel to the crystallographic axes a, b, and c, respectively. The local relation between the orbital magnetic moment $\mathbf{M}_L^i$ and the spin magnetization direction $\mathbf{e}=(\cos\theta\sin\phi,\sin\theta\sin\phi,\cos\theta)$ on each vanadium site i can generally be written as $M_{L\alpha}^i=\mathcal{L}_{\alpha\beta}^i e_\beta$, where the matrix $\mathcal{L}_{\alpha\beta}^i$ determines the orbital magnetic moment induced by the spin-orbit interaction. We apply the mentioned symmetry operations to the matrix $\mathcal{L}_{\alpha\beta}^i$ to obtain averaged matrices $\mathcal{L}_{\alpha\beta}=\Sigma_{i=1}^4\mathcal{L}_{\alpha\beta}^i$ for the C- and G-type spin ordering, respectively:

$$\mathcal{L}^C=4\begin{pmatrix} 0 & \mathcal{L}_{xy}^1 & 0 \\ \mathcal{L}_{yx}^1 & 0 & 0 \\ 0 & 0 & 0 \end{pmatrix}, \quad \mathcal{L}^G=4\begin{pmatrix} 0 & 0 & \mathcal{L}_{xz}^1 \\ 0 & 0 & 0 \\ \mathcal{L}_{zx}^1 & 0 & 0 \end{pmatrix}.$$

The corresponding net orbital magnetic moments are

$$C: \quad \mathbf{M}_L^C=4(\mathcal{L}_{xy}^1\sin\theta\sin\phi,\mathcal{L}_{xy}^1\sin\theta\cos\phi,0),$$

$$G: \quad \mathbf{M}_L^G=4(\mathcal{L}_{xz}^1\cos\theta,0,\mathcal{L}_{zx}^1\sin\theta\cos\phi).$$

The orbital magnetic moment $\mathbf{M}_L$ has the same symmetry as the gyration vector $\mathbf{g}$,[26] which determines the antisymmetric part of the dielectric tensor, $\varepsilon_{\alpha\beta}^a=ie_{\alpha\beta\gamma}g_\gamma$, responsible for mageto-optical effects.[27] Here $e_{\alpha\beta\gamma}$ is the unit antisymmetric tensor. In the polar measurement geometry discussed here, components of the vector g_α and, correspondingly, components of $\mathbf{M}_L$ define the orientation of the magnetic field H for which observation of Kerr effect is possible.

For the G-type spin order, the structure of $\mathbf{M}_L^G$ suggests that the polar Kerr effect can exist for $H||a$ if spins are parallel to the c axis and for $H||c$ if spins are aligned along the a axis. If the spins are along the b axis, $\mathbf{M}_L^G$ and the corresponding Kerr effect are zero. This does not exclude the possibility for the second, weaker, type of Kerr effect, which is directly related to the spin canting. It should be emphasized here that Kerr rotation due to orbital magnetic moments can exist even if the spins are exactly antiferromagnetically aligned.[25] Our observation of a substantial magneto-optical effect only for $H||a$ shows that spins in the low-temperature phase of YVO_3 are aligned along the c axis. This agrees with neutron scattering measurements.[4] The weak structure at 1.8 and 2.2 eV is most probably the spin canting effect.

The C-type spin order as seen from the $\mathbf{M}_L^C$ angular dependence allows a magneto-optical activity, only if spins are aligned in the ab plane. The small magnitude of the experimentally observed MOKE above 80 K compared to the low-temperature phase suggests that the spins are aligned along the c axis. In this case, $\mathbf{M}_L^C$ is zero for any orientation of H, and the Kerr effect substantially decreases, in agreement with our experimental observations. This result contradicts the neutron data, where a substantial spin component along the b axis is observed[4]. This, however, can reflect another important property of YVO_3. As was shown in Ref. 28, G-type antiferromagnetic orbital order in the form proposed by Ren *et al.*[2] suppresses the orbital magnetic moment. This can be the reason why no substantial Kerr rotation was observed for the C-type spin order. This conclusion requires that the on-site magnetic moment in the G-type orbital order be reduced from $2\mu_B$ to $1.1\mu_B$,[4] not due to the orbital magnetic moment, but due to a mixture of $S_z=1$ and $S_z=0$ $^3T_{1g}$ states, in agreement with the conclusion obtained in the previous section.

VI. CONCLUSIONS

The analysis of the YVO_3 phonon spectra revealed three different phases. The orthorhombic *Pbnm* structure exists down to 200 K. At 200 K there is a second-order phase transition to a lower-symmetry structure. The orthorhombic *Pbnm* crystal symmetry is restored through a first-order phase transition below 74 K. The most probable structure in the intermediate phase is the monoclinic $Pb11$, where the VO_6 octahedra form a dimerized chain along the c axis. Nevertheless, the possibility of a triclinic $P\overline{1}$ symmetry cannot be excluded completely.

YVO_3 is a Mott-Hubbard insulator with an optical gap of 1.6 eV. There are three optical bands with energies 1.8, 2.4, and 3.3 eV, which we identify with the intervanadium transitions from the $^3T_{1g}$ ground state to the $^4A_{2g}$, $^2E_g+{}^2T_{1g}$, and $^2T_{2g}$ states. These d-d excitations are followed by the charge-transfer transitions at 4 eV. The band gap structure is in agreement with the LSDA+U calculations. The d bands revealed a strong temperature dependence. Using a model which includes only the nearest-neighbor transitions, we found that the observed temperature dependence disagrees with the simple antiferromagnetic spin ordering. This indicates that orbital ordering phenomena are responsible for the observed temperature variations. However, the commonly considered $|xy,xz|/|xy,yz|$ orbital order seems also inconsistent with our data, if we assume a fully polarized on-site state.

We observed two types of magneto-optical effects. A small net magnetic moment due to the uncompensated spin moments induces a weak Kerr rotation of the order of $\sim 0.01°$. The effect exists in all phases below the magnetic ordering temperature and for all active optical transitions. A strong Kerr effect appears as a consequence of the low crystallographic symmetry and ferromagnetic ordering of the orbital magnetic moments. A Kerr rotation of the order of ~0.1° was found in the low-temperature phase for the highest *d-d* transition band. It follows from symmetry considerations that the spin magnetic moment is aligned along the *c* axis in both magnetic structures. However, this conclusion for the *C*-type AFM spin arrangement can be affected by the accompanying orbital order.

ACKNOWLEDGMENTS

We acknowledge useful discussion with G. R. Blake. We thank H. J. Bron for his help with sample preparation. This research was supported by The Netherlands Foundation for Fundamental Research on Matter (FOM) with financial aid from the Nederlandse Organisatie voor Wetenschappelijk Onderzoek (NWO).

---

*Present address: NSRIM Institute, University of Nijmegen, Toernooiveld 1, 6525 ED Nijmegen, The Netherlands. Electronic address: tsvetkov@sci.kun.nl

†On leave from Jurusan Fisika, Institut Teknologi Bandung, Jl. Ganesha 10, Bandung 40132, Indonesia.

[1] K.I. Kugel and D.I. Khomskii, Zh. Éksp. Teor. Fiz. **64**, 1429 (1973) [Sov. Phys. JETP **37**, 725 (1973)].

[2] Y. Ren, T.T.M. Palstra, D.I. Khomskii, E. Pellegrin, A.A. Nugroho, A.A. Menovsky, and G.A. Sawatzky, Nature (London) **396**, 441 (1998).

[3] H. Kawano, H. Yoshizawa, and Y. Ueda, J. Phys. Soc. Jpn. **63**, 2857 (1995).

[4] G.R. Blake, T.T.M. Palstra, Y. Ren, A.A. Nugroho, and A.A. Menovsky, Phys. Rev. B **65**, 174112 (2002).

[5] D.B. Rogers, A. Ferretti, D.H. Ridgley, R.J. Arnott, and J.B. Goodenough, J. Appl. Phys. **37**, 1431 (1966).

[6] V.G. Zubkov, A.S. Borukhovich, G.V. Bazuev, I.I. Matveenko, and G.P. Shveikin, Sov. Phys. JETP **39**, 896 (1974).

[7] G.R. Blake, T.T.M. Palstra, Y. Ren, A.A. Nugroho, and A.A. Menovsky, Phys. Rev. Lett. **87**, 245501 (2001).

[8] C. Ulrich, G. Khaliullin, J. Sirker, M. Reehuis, M. Ohl, S. Miyasaka, Y. Tokura, and B. Keimer, cond-mat/0211589 (unpublished).

[9] Y. Ren, T.T.M. Palstra, D.I. Khomskii, A.A. Nugroho, A.A. Menovsky, and G.A. Sawatzky, Phys. Rev. B **62**, 6577 (2000).

[10] M. Schubert, T.E. Tiwald, and C.M. Herzinger, Phys. Rev. B **61**, 8187 (2000), and references therein.

[11] K. Sato, H. Hongu, H. Ikekame, Y. Tosaka, M. Watanabe, K. Takanashi, and H. Fujimori, Jpn. J. Appl. Phys., Part 1 **32**, 989 (1993).

[12] D.L. Rousseau, R.P. Bauman, and S.P.S. Porto, J. Raman Spectrosc. **10**, 253 (1981).

[13] A.A. Tsvetkov, F.P. Mena, Y. Ren, I.S. Elfimov, P.H.M. van Loosdrecht, D. van der Marel, A.A. Nugroho, A.A. Menovsky, and G.A. Sawatzky, Physica B **312**, 783 (2002).

[14] I.S. Smirnova, Physica B **262**, 247 (1999).

[15] S. Miyasaka, Y. Okimoto, and Y. Tokura, J. Phys. Soc. Jpn. **71**, 2086 (2002).

[16] J. Zaanen, G.A. Sawatzky, and J.W. Allen, Phys. Rev. Lett. **55**, 418 (1985).

[17] M. Kasuya, Y. Tokura, T. Arima, H. Eisaki, and S. Uchida, Phys. Rev. B **47**, 6197 (1993).

[18] T. Arima, Y. Tokura, and J.B. Torrance, Phys. Rev. B **48**, 17 006 (1993).

[19] O.K. Andersen, Phys. Rev. B **12**, 3060 (1975).

[20] V.I. Anisimov, J. Zaanen, and O.K. Andersen, Phys. Rev. B **44**, 943 (1991).

[21] H. Sawada and K. Terakura, Phys. Rev. B **58**, 6831 (1998).

[22] For example, if we maximize the spin magnetic moment, we obtain that the $|xz,yz|$ orbitals should be always occupied on all vanadium sites. This gives correct intensity changes for the all bands and all axes.

[23] I.V. Solovyev, N. Hamada, and K. Terakura, Phys. Rev. Lett. **76**, 4825 (1996).

[24] L.M. Sandratskii and J. Kübler, Phys. Rev. Lett. **76**, 4963 (1996).

[25] I.V. Solovyev, Phys. Rev. B **55**, 8060 (1997).

[26] Y.A. Uspenskii, E.T. Kulatov, and S.V. Halilov, Phys. Rev. B **54**, 474 (1996).

[27] D.L. Landau and E.M. Lifshitz, *Electrodynamics of Condensed Media* (Pergamon, New York, 1960).

[28] T. Jo, J. Phys. Soc. Jpn. **72**, 155 (2003).